AIAA AVIATION Forum
12-16 June 2023, San Diego, CA and Online
AIAA AVIATION 2023 Forum

10.2514/6.2023-4189

A Two-Dimensional Mode-Matching Technique for Wake-Interaction Tonal Noise Including Rotor-Stator Coupling

Léo Girier* and Michel Roger†
Univ Lyon, École Centrale de Lyon, INSA Lyon, Université Claude Bernard Lyon I, CNRS, Laboratoire de Mécanique des Fluides et d'Acoustique, UMR 5509, 36 Avenue Guy de Collongue, F-69134, Écully, France

Anthony Lafitte‡ and Hélène Posson§
Safran Aircraft Engines, Rond Point René Ravaud - Réau, 77550, Moissy-Cramayel, France

Noise generated by the impingement of rotor wakes on guide vanes is still widely studied in the context of turbofan noise. However, analytical models are often limited to an isolated stator made of flat-plate vanes, neglecting the presence of the rotor. The present work proposes an iterative procedure based on successive applications of a mode-matching technique on the stator and the rotor to model the acoustically coupled rotor-stator system, including vane camber. This allows one to study the "shielding" effect of the rotor and the occurrence of inter-stage trapped modes, in order to better predict the relative balance between upstream and downstream sound powers, as well as modal and frequency contents. The influence of inter-stage distance and rotor rotational speed on sound generation and propagation is investigated in this paper. It appears that the additional scattering by the rotor can have a significant impact on the emerging tones by redistributing sound through frequencies. The ratio of downstream to upstream acoustic power tends to increase compared to the single stator computation, as previously reported in the literature, even if an artificial swirl is imposed upstream of the compressor stage in the present study. However, the total sound power with and without the rotor scattering remains the same in the performed test cases.

Downloaded by Christophe Bogey on October 10, 2023 | http://arc.aiaa.org | DOI: 10.2514/6.2023-4189

I. Nomenclature

BPF	=	Blade Passing Frequency
LE	=	Leading Edge
TE	=	Trailing Edge
U	=	Mean velocity in the stationary reference frame
W	=	Mean velocity in the rotating reference frame
Ω	=	Rotation rate
M	=	Mach number
D	=	Mean Density
P	=	Mean Pressure
C	=	Mean sound speed
R	=	Radius of the unwrapped cut
l	=	Chord length
a	=	Inter-vane channel height / angular spacing
d	=	Inter-stage distance
B	=	Rotor blades number
V	=	Stator vanes number
n	=	BPF wake harmonic
m	=	Acoustic incident azimuthal order
s	=	Scattering index

*Postdoctoral Researcher, Laboratoire de Mécanique des Fluides et d'Acoustique, leo.girier@ec-lyon.fr.
†Professor, Laboratoire de Mécanique des Fluides et d'Acoustique.
‡Aeroacoustics Engineer, Safran Aircraft Engines.
§Aeroacoustics Engineer, Safran Aircraft Engines.

Copyright © 2023 by Léo Girier, Michel Roger, Anthony Lafitte and Hélène Posson .
Published by the American Institute of Aeronautics and Astronautics, Inc., with permission.

ω = Angular frequency
u = Velocity
ρ = Density
p = Pressure
c = Sound speed
ϕ = Velocity potential
u^R = Vortical velocity
u_K^R = Kutta vortical velocity
$\mathcal{P}$ = Acoustic power
SWL = Sound Power Level

II. Introduction

Despite the drop in air traffic since the Covid-19 outbreak and a growing societal concern regarding aircraft pollution, air traffic in Europe is recovering and might already return to its 2019 value by 2024*. Aircraft noise pollution therefore remains an important societal problem. In this context, it is crucial to reduce engine noise, which remains one of the major sources of overall aircraft noise, particularly during take-off. A study made in the early century, on typical long-range four-engine aircraft [1], pointed out that the noise generated by the fan stage has become as important as jet noise during take-off and is also crucial in approach condition. Reducing fan-related noise then appears as one of the main lever to reduce the overall aircraft noise emission. The present work focuses on the modeling of fan-related noise, and more specifically on rotor-stator wake-interaction tonal noise.

Most of the analytical studies on wake-interaction tonal noise have been devoted to the improvement of the disturbance and cascade-response models. One major flaw of these models is that they are often limited to a single cascade of vanes interacting with prescribed wakes coming from upstream, neglecting the effect of sound transmission and reflection by the rotor. Typically, trapped modes can develop between the rotor and the stator, and the modal and frequency scattering of stator noise by the rotor redistributes noise to other harmonics of the Blade Passing Frequency (BPF). Topol et al. [2] demonstrated a significant impact of noise reflection from the rotor in full-scale engine measurements. In particular, data from a high bypass ratio engine showed evidence of mode trapping and frequency scattering. A surge at $3 \times$ BPF was observed and attributed to the tone $1 \times$ BPF that turned cut-on in the inter-stage while remaining cut-off outside, allowing the rotor to scatter its energy to other frequencies. Topol et al. [2] were among the first to propose a correction for the aft noise, including rotor reflection and frequency scattering in a one-way coupling. Kaji and Okazaki did pioneering works on the rotor-stator interaction in 1970, but their model was restricted to a single frequency and did not include the swirl effect in the inter-stage. In order to account for the full rotor-stator coupling with swirl, Hanson [3, 4] developed a fully coupled methodology and applied it to a two-dimensional rotor-stator stage. The scattering coefficients of the rotor and of the stator were computed from a cascade-response theory developed by Smith [5], based on the Wiener-Hopf technique, and gathered in a global scattering matrix to be inverted. Hanson showed that trapped modes are more likely to occur in the inter-stage because of the impact of swirl on the inter-stage cut-on condition. Hanson [6] focused on the effects of mode and frequency scattering by a rotor and a stator separately, to break down some of the reflection and transmission phenomena occurring in a rotor-stator stage. One of the most noticeable results was that modes reflected by the rotor could have more energy than the incident mode that generated them. This phenomenon was attributed to the rotor motion, increasing the energy of the modes scattered at higher frequencies. Modes scattered without frequency shift did not show power increase but the analysis was limited to incident modes at $1 \times$ BPF.

The purpose of the present work is to address the interaction with a mode-matching technique, presented as an alternative to other approaches, able to include realistic design parameters. The mode-matching technique, introduced some decades ago, has recently seen a revival of interest. It already showed promising capabilities to model sound generation and propagation in isolated stator stages. For a comprehensive review, the reader can refer, for instance, to the work by Bouley and co-authors [7, 8]. An extension to cascades of thick-walled channels is also possible, as shown by Oulmi et al. [9], or to cambered vanes, ensuring a continuous deviation of the flow, with some increase of the mathematical efforts, as discussed by Girier et al. [10, 11]. More recently, a mode-matching based model has been developed to study sound generation and propagation in a coupled system consisting of two stationary periodic rows of cooling channels in a railway ventilation system [12]. The model has also been extended to rotating rows [13]. The present work is similar in essence, combining the multiple-scattering formulation with the cambered-vane extension. In

*sources: EUROCONTROL/Forecast Update 2023-2029, March 2023 (https://www.eurocontrol.int/publication/eurocontrol-forecast-update-2023-2029) and IATA/Tourism Economics Air Passenger Forecast, March 2022

Downloaded by Christophe Bogey on October 10, 2023 | http://arc.aiaa.org | DOI: 10.2514/6.2023-4189

Hanson's works [3, 4, 6], alternatively, the actuator disk theory was used to model jumps in the flow conditions at the rotor leading-edge and stator trailing-edge interfaces. Due to the importance of the flow deviation in the occurrence of trapped modes, it seems interesting to develop a model with continuous flow evolution through the entire rotor-stator stage for more reliable predictions.

In summary, wake-interaction tonal noise in a coupled rotor-stator system has only been modeled analytically with flat blades/vanes and discontinuous flow conditions in the past, motivating extensions. A fast analytical prediction tool could be of great value to get a better understanding of fan noise in early design steps in an engineering context. For that purpose, a two dimensional mode-matching based model for fully coupled rotor-stator wake-interaction tonal noise is proposed, in the continuity of the aforementioned recent works.

The outline of the paper is as follows. The mathematical formulation and the mode-matching technique background are presented in section III. In section IV, the validity of the method is first demonstrated by analyzing the acoustic power balance with an incident acoustic wave scattered by a stator-stator system, and a rotor-alone configuration. Computations of sound generation and propagation in a rotor-stator stage are conducted in section V alongside parametric studies on various flow and geometrical parameters. Finally, some limitations and possible improvements of the current model version are discussed in section VI and concluding remarks are drawn.

Downloaded by Christophe Bogey on October 10, 2023 | http://arc.aiaa.org | DOI: 10.2514/6.2023-4189

III. Mathematical Formulation

A. Mode-Matching Technique

1. General Principle

The mode-matching technique is explained for the case of an incident acoustic wave, for which an illustrative scheme is given in Fig. 1, without stagger or camber. Detailed explanations of how to add stagger and camber can be found in Refs. [10, 11]. An incident acoustic mode, described by its velocity potential ϕ_i, is scattered at the cascade Leading-Edge (LE) interface, generating reflected modes ϕ_r and transmitted modes ϕ_d in the channels. The latter are then scattered at the Trailing-Edge (TE) interface, giving rise to reflected channel modes ϕ_u and transmitted modes ϕ_t. Hard-walled boundary conditions at the walls of the inter-vane channels and periodic boundary conditions in the y-direction are imposed.

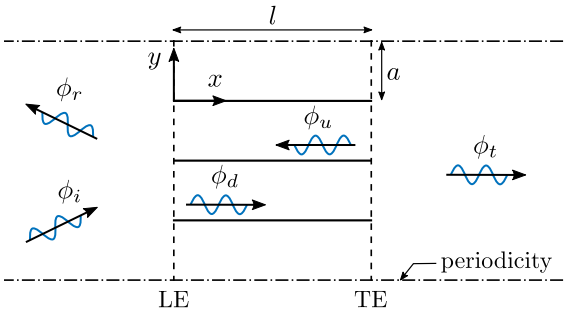

Fig. 1 Scattering of an incident acoustic wave by a linear cascade of flat vanes.

The mode-matching technique can be described in three steps: partitioning, solving, and matching. The *partitioning* consists in dividing the domain into different sub-domains in which the boundary conditions are uniform and the wave equation separable, allowing a solution on a local modal basis. In Fig. 1, the sub-domains are the upstream medium, each inter-vane channel and the downstream medium. The *solving* step provides the wavenumbers and modal shapes of the scattered waves in each sub-domain, based on an appropriate Helmholtz equation. For simple geometries such as in Fig. 1, these wavenumbers and eigenfunctions are analytically known. Finally, the only remaining unknowns are the modal coefficients of the waves. They are defined by *matching* the different modal solutions at both leading-edge and trailing-edge interfaces. To do so, continuity equations specific to the problem are used to build a set of equations on the modal coefficients, which can be solved by matrix inversion. The equations that need to be satisfied through a compressor stage are derived from the classical conservation equations (mass and energy) applied to an adiabatic lossless turbomachine [14]. In this context, the mass conservation is equivalent to mass-flow continuity and the energy conservation is expressed through stagnation enthalpy. The solving and matching steps are detailed in what follows.

2. Solving Step: Wave Equation in the Sub-Domains

Compressibility is accounted for in the Euler equations and the *ideal gas* law is used. Furthermore, the fluid is considered *inviscid* and the flow *isentropic*. Defining the following quantities: ρ^* as the density, $\mathbf{u}^*$ as the velocity, c^* as the sound speed and p^* as the pressure, the flow is then split up into a steady component (time average) and its fluctuations. The fluctuating part varies harmonically in time, with angular frequency ω, and is assumed to be small enough to allow linearization. Thus, the decomposition reads

$$[\mathbf{u}^*, \rho^*, p^*, c^*] = [\mathbf{U}, D, P, C] + [\mathbf{u}, \rho, p, c]\, \mathrm{e}^{-\mathrm{i}\omega t}. \tag{1}$$

The fluctuating velocity $\mathbf{u}$ can be expressed as the sum of independent acoustic and vortical motions according to the analysis of Chu & Kovásznay [15] at leading order. The fundamental theorem of vector calculus states that $\mathbf{u}$ can be decomposed into the sum of a rotational-free field $\nabla\phi$ and a divergence-free field $\mathbf{u}^R$, which are associated, in this case, to the acoustic and vortical motions, respectively. Thus, the fluctuating velocity $\mathbf{u}$ reads

$$\mathbf{u} = \nabla\phi + \mathbf{u}^R. \tag{2}$$

Defining the pressure field as

$$p = -D\left(-\mathrm{i}\omega\phi + \mathbf{U}\cdot\nabla\phi\right), \tag{3}$$

the vortical field $\mathbf{u}^R$ is then uniquely defined by

$$(-i\omega + \mathbf{U}\cdot\nabla)\mathbf{u}^R = 0, \tag{4}$$

where the second-order vortical-acoustic and vortical-vortical coupling terms are neglected (see for example Ref. [11] for detailed explanations). The pressure field, on the other hand, is given by the following homogeneous compressible wave equation

$$D(-i\omega + \mathbf{U}\cdot\nabla)\left[\frac{1}{C^2}(-i\omega + \mathbf{U}\cdot\nabla)\phi\right] - \nabla\cdot(D\nabla\phi) = 0. \tag{5}$$

3. Matching Step: Jump Conditions at the Interfaces

The mass conservation at an interface between a sub-domain 1 and a sub-domain 2, equivalent to the mass-flow conservation through the interface, reads

$$\left[\frac{p}{Z}M_x^2 + M_x u_x\right]_1^2 = 0, \tag{6}$$

where the brackets denote the difference of the quantity between both sides of the interface, $Z = DC$ and $M_x = U_x/C$ (the subscript x referring to the projection along the corresponding axis of Fig. 1). The conservation of stagnation enthalpy [14] states that

$$\left[\frac{p}{Z} + M_x u_x + M_y u_y\right]_1^2 = 0. \tag{7}$$

Writing U as the norm of the mean velocity and Ψ as the angle it makes with the direction perpendicular to the interface, the x-axis in Fig. 1, allows one to express the mean velocity components as $U_x = U\cos\Psi$ and $U_y = U\sin\Psi$. Equation (7) is then recast as

$$\left[\frac{p}{Z} + M_x\left(u_x + u_y\tan\Psi\right)\right]_1^2 = 0. \tag{8}$$

Combining Eq. (6) and (8) allows one to recover the conservation of the fluctuating pressure p and fluctuating axial velocity u_x, commonly used in mode-matching procedures, but only for the particular case where the mean flow is perfectly perpendicular to the matching interface, i.e. when $\Psi = 0$. In general, when $\Psi \neq 0$, new variables need to be introduced to ensure the conservation of mass-flow and stagnation enthalpy through the interface. These conservative variables are written Γ_1 and Γ_2 in the following, and are gathered into a vector $\Gamma_\gamma = (\Gamma_{1\gamma}, \Gamma_{2\gamma})$, where the index γ stands either for the incident (i), reflected annular (r), transmitted annular (t), downstream-propagating channel (d) or upstream-propagating channel (u) field (see Fig. 1). The matching equations then read

$$\begin{cases} \Gamma_i + \Gamma_r = \Gamma_d + \Gamma_u & \text{at LE,} \quad (9) \\ \Gamma_d + \Gamma_u = \Gamma_t & \text{at TE.} \quad (10) \end{cases}$$

In case of an incident acoustic wave, the velocity field is purely potential. The first variable is chosen as the velocity potential $\Gamma_1 = \phi$ and the second one as a combination of axial and transverse velocities $\Gamma_2 = \beta_x^2 u_x - M_x M_y u_y$, where $\beta_x = \sqrt{1 - M_x^2}$. If a vortical wave is present, as for sound generation by wake impingement and/or when a Kutta condition is imposed, then $\Gamma_1 = \beta_x^2 p/Z + M_y u_y$, whereas Γ_2 remains unchanged.

Downloaded by Christophe Bogey on October 10, 2023 | http://arc.aiaa.org | DOI: 10.2514/6.2023-4189

B. Rotor-Stator Back-and-Forth Iterative Procedure

1. Recursive Algorithm

The procedure begins by an iteration of direct noise generation or acoustic scattering on the stator, depending on the vortical or acoustic nature of the incident wave, respectively. This produces the first set of acoustic modes. A recursive algorithm is then called to iterate back-and-forth between the secondary cascade (rotor) and primary cascade (stator) until a convergence on the modal coefficients is reached. To do so, a filter is applied at each step on the scattered acoustic modes to retain only the most significant ones for the next iteration. A mode is filtered out if its amplitude is at least two orders of magnitude lower than a reference amplitude. This reference is chosen as the initial wave in the case of acoustic scattering, or the strongest acoustic mode produced by the initial iteration in the case of wake interaction. The recursive algorithm iterates on each mode independently by virtue of linearity, so a graph tree is constructed gradually. A branch reaches an endpoint when the filter retains no modes. All coefficients and acoustic powers are finally summed up together on mode order and frequency for the annular domains, and also on inter-vane phase shift for the channel modes. The algorithm is implemented in the MATLAB environment and runs in a few seconds on a personal laptop for a given disturbance component.

2. Acoustic Power

On top of the recursive algorithm, radiated acoustic powers are computed at each iteration based on Goldstein's formulation [16]. This is used as an indicator of energy conservation *a posteriori*, but the convergence of the algorithm is solely based on the modal coefficients. For rotor-stator sound generation, a global power balance is not accessible for now, because the hydrodynamic power carried by the vortical gust is not estimated. However, for validation purposes, cases of acoustic scattering are presented in section IV.A and IV.B, for which the global sound power balance can be computed.

IV. Preliminary Analyses on the Acoustic Power Balance

A. Stator-Stator System with Incident Acoustic Wave

The developed model presents two new additions compared to the aforementioned literature that need to be investigated beforehand: the recursive algorithm coupling the cascades and the rotating motion. The latter has, in fact, already been modeled and studied, essentially by Hanson [6], but lacks some physical understanding. In a first instance, the validity of the recursive procedure is tested with a system composed of two stators excited by an incident acoustic wave. The algorithm should converge in terms of modal coefficients and the acoustic power balance should remain within 1% error. A schematic view of the problem is depicted in Fig. 2. A primary cascade of $V_1 = 23$ vanes and a secondary cascade of $V_2 = 17$ vanes are separated by a distance $d/l_2 = 1.5$. Considering a radius of $R = 22.35$ cm, the two sets of geometrical parameters are defined by $a_{1,2}/R = 2\pi/V_{1,2}$ and $l_{1,2} = \sigma_{1,2}a_{1,2}$, where the solidity values are $\sigma_1 = 1.5$ and $\sigma_2 = 1.2$. The incident acoustic wave is defined by its azimuthal order $m = -7, 5, 11$ and its dimensionless frequency $\omega d/\pi C$ ranges from 2 to 7 approximately. This range of frequencies and azimuthal orders will give a sufficient basis of validation to build confidence in the results obtained later on for wake-interaction.

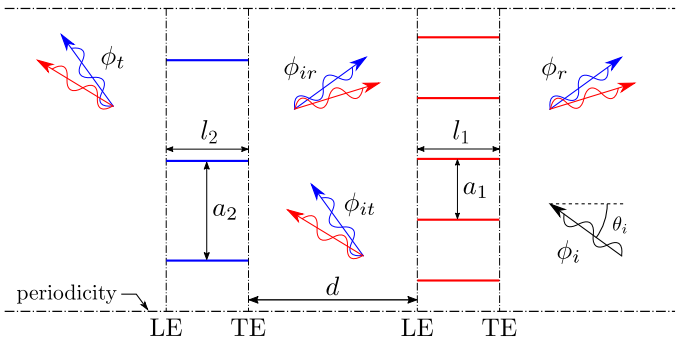

Fig. 2 Sketch of the stator-stator system with an incident acoustic wave coming from the right. The colors are here to remind that the modes are scattered with the periodicity of both cascades.

Downloaded by Christophe Bogey on October 10, 2023 | http://arc.aiaa.org | DOI: 10.2514/6.2023-4189

Fig. 3 shows the acoustic power balance $(\mathcal{P}_i + \mathcal{P}_r - \mathcal{P}_t)/\mathcal{P}_i$[†] against the angular frequency for the different incident azimuthal orders. The conservation of the acoustic power is achieved across the whole frequency range, except at some specific frequencies.

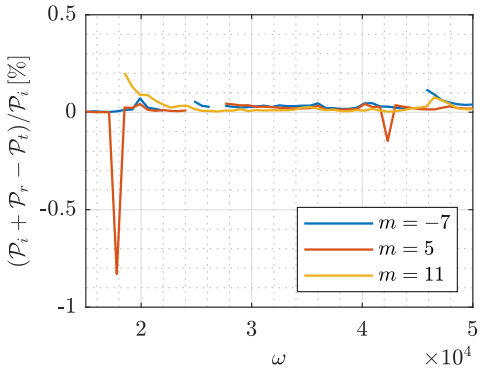

Fig. 3 Acoustic power balance against angular frequency for different mode orders m.

Looking at Fig. 4a, which represents the relative reflected and transmitted powers for $m = 5$, a resonance seems to take place in the missing frequency range. It is known from previous studies [11] that at resonant frequencies the method becomes much more sensitive to modal truncation. In absence of dissipating mechanism, it might be impossible to converge to a power-conserving solution. Adding a mean flow of Mach number $M = 0.45$ in the opposite direction to that of the incident wave is sufficient to attenuate the resonance and allows the solver to converge, even without imposing a Kutta condition in this case (see Fig. 4b). As expected, the resonant frequencies are shifted in the low-frequency range. Furthermore, the second resonance, not observable before, is now clearly evidenced. Note that the total acoustic power is still well conserved. A computation on the primary cascade alone, not presented in this paper, has shown that both resonant frequencies in the case $m = 5$ are due to the primary cascade, neither to the secondary cascade nor to the inter-stage area.

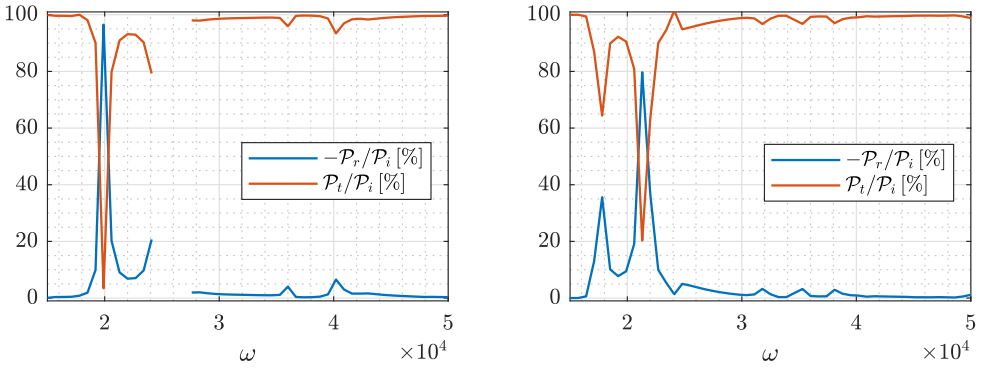

Fig. 4 Relative reflected and transmitted sound powers without flow (a) and with flow of Mach number $M = 0.45$ in the opposite direction to that of the incident wave (b).

The test demonstrates the relevance and the validity of the iterative procedure for a tandem of stationary cascades. The next section is naturally devoted to the case of a rotating cascade alone, before going to the rotor-stator case.

[†]The acoustic power is defined as the integral over the duct height of the energy flux projected on the horizontal axis (see Ref. [16]), and thus is negative for upward-traveling waves and positive for downward-traveling waves.

Downloaded by Christophe Bogey on October 10, 2023 | http://arc.aiaa.org | DOI: 10.2514/6.2023-4189

Downloaded by Christophe Bogey on October 10, 2023 | http://arc.aiaa.org | DOI: 10.2514/6.2023-4189

B. Rotor Alone with Incident Acoustic Wave

This time, a rotating cascade is examined alone in order to emphasize on the sound-power imbalance due to the motion of a scattering surface, which will help analyze sound power outputs in the rotor-stator case. The problem is sketched in Fig. 5, where the absolute mean velocity is noted U, the relative mean velocity W and the rotation rate Ω. Note that W is always aligned with the blades and $M = U/C$ is fixed to 0.55, so that $|W|$ changes when the rotation rate varies as $|W|^2 = |U|^2 - |\Omega R|^2$. The cascade is made of $B = 31$ blades with a chord-to-gap ratio $\sigma_2 = 1.2$, and the acoustic excitation is defined by $m = 16$ and $\omega a/\pi C = 1.5$. The radius of the unwrapped cut is taken as $R = 22.35$ cm.

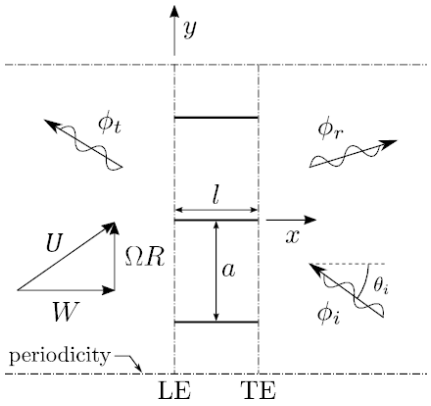

Fig. 5 Sketch of the model rotor cascade with an incident acoustic wave, featuring the velocity triangle.

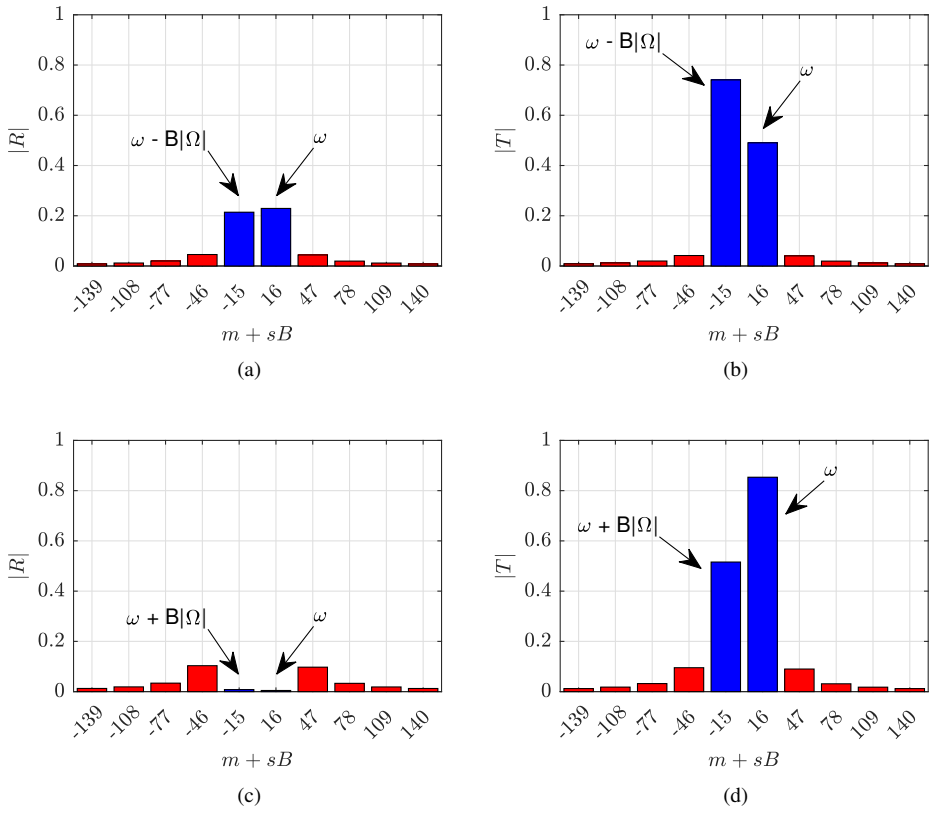

Fig. 6 Reflected (a-c) and transmitted (b-d) modal contents for a rotational Mach number of $M_\Omega = 0.4$ (first line) and $M_\Omega = -0.4$ (second line).

The scattering of this incident mode generates only two cut-on modes: $m + sB = 16$ ($s = 0$) and $m + sB = -15$ ($s = -1$). Fig. 6a and 6b display the reflected and transmitted modal contents, respectively, for a rotational Mach number $M_\Omega = \Omega R/C = 0.4$, while Fig. 6c and 6d do the same for the opposite rotation $M_\Omega = -0.4$. In the first case, the cascade scatters the incident mode into the opposite direction to that of its rotation ($s\Omega < 0$), which leads to a lower frequency $\omega + sB\Omega = \omega - B|\Omega|$. In the second case, the rotating motion is reversed and the scattered mode $m + sB = -15$ is then scattered at a higher frequency: $\omega + B|\Omega|$.

The relative reflected and transmitted acoustic powers are plotted against the rotational Mach number in Fig. 7a. What is noticeable from this plot is that the transmitted power is greater than the incident power for $M_\Omega < 0$, and then drops for $M_\Omega > 0$ without being compensated by the reflected power. A closer look on the sound power balance is given in Fig. 7b. An increased scattered power is found when the mode -15 is scattered at a higher frequency ($M_\Omega < 0$), whereas a decrease is found when this mode is scattered at a lower frequency ($M_\Omega > 0$). This is in remarkable agreement with the theory of Hanson [6], who made a quick mathematical derivation based on Goldstein's energy flux [16] expressed in the relative and absolute reference frames. According to Hanson, this results from the cascade motion, giving or taking energy from the scattered waves[‡]. The rotor does work on the acoustic field, since there is no other way to exchange energy in the model. This is because the conservation of stagnation enthalpy in the rotating frame of reference is equivalent to the conservation of rothalpy. The rothalpy, for rotational enthalpy, is the physical quantity conserved through the rotor in this case, as suggested by thermodynamics [14]. It seems that when the rotor "pulls" the incident mode in the same direction as its rotation ($s\Omega > 0$), it gives part of its kinetic energy to the scattered mode. On the other hand, when it "pushes" the incident mode in the opposite direction to that of its rotation ($s\Omega < 0$), the rotor takes part of the acoustic energy of the scattered mode.

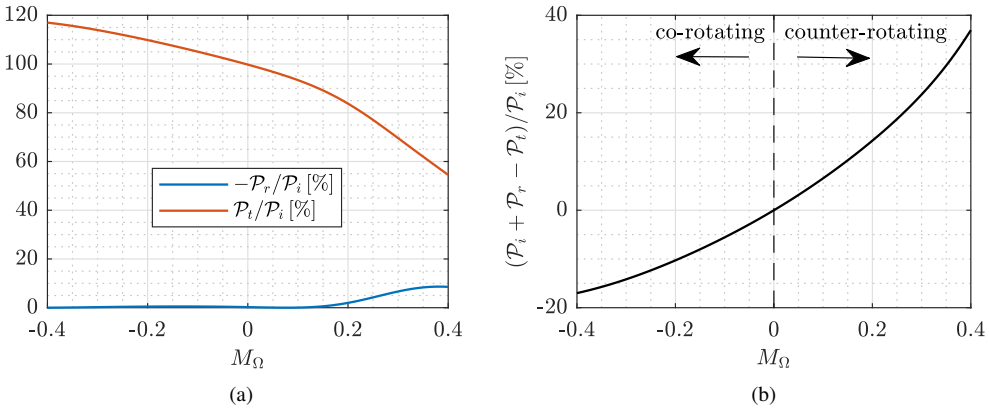

Fig. 7 Relative reflected and transmitted acoustic powers (a) and power acoustic balance (b) against rotational Mach number: the co- and counter-rotating indications refer to the scattered mode -15.

V. Wake-Interaction Noise Results

A. Rotor-Stator vs. Stator Alone

Now that energy conservation of the recursive algorithm has been assessed in the test case of section IV.A, and that the power imbalance due to the rotor scattering has been explained in section IV.B, the complete and fully coupled rotor-stator system is studied in this section, and results are compared with the stator-alone case. Analyses of instantaneous pressure maps, modal contents and sound power outputs are performed in what follows. A sketch of the system is represented in Fig. 8. The stator is made of $V = 31$ cambered vanes with a camber angle of $\Psi = 20°$ and a stagger angle of $\Psi/2 = 10°$. The incoming mean flow Mach number is $M = U/C = 0.4$, with artificial swirl upstream of the stage. This is due to the use of flat rotor blades, because blade camber is not currently available in the code, and the need for a continuous mean flow evolution. The rotor is made of $B = 16$ zero-stagger flat blades

[‡]Notice that computations performed with no frequency shift (no scattered mode $s \neq 0$), not presented here, have shown no power imbalance. Hanson [6] also mentioned the same outcome.

Downloaded by Christophe Bogey on October 10, 2023 | http://arc.aiaa.org | DOI: 10.2514/6.2023-4189

rotating in the positive direction at a rate $M_\Omega = \Omega R/C = M \sin\Psi \simeq 0.137$, and the relative mean flow Mach number is $M_r = W/C = M \cos\Psi \simeq 0.376$. Compared to section IV, a Kutta condition is now applied to the trailing edges of both cascades, enforcing a zero pressure jump and adding an infinitely-thin vortical sheet downstream, the velocity field of which is noted u_K^R. Sound generation is computed for the 5$^{\text{th}}$ BPF wake harmonic $n = 5$ and the amplitude of the vortical disturbance is fixed to unity in all test cases: $|u_i^R| = 1$. No wake evolution is modeled from the rotor TE to the stator LE.

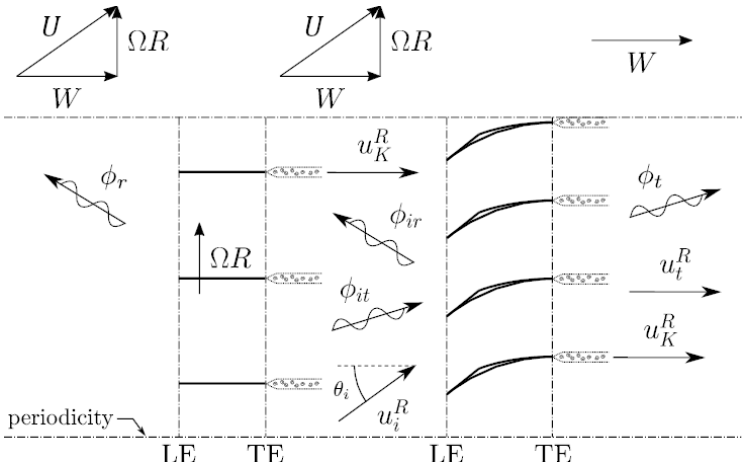

Fig. 8 Sketch of the rotor-stator system with an incident vortical wave and a Kutta condition imposed at the trailing edges of both cascades, featuring the velocity triangles.

The generated pressure field is displayed in Fig. 9a, and without the rotor in Fig. 9b. A strong interaction is visible in the inter-stage area in Fig. 9a, as well as a disturbed wave-front upstream that indicates a multimodal propagation. In the stator-alone scenario (Fig. 9b), a single mode propagates upstream. By looking at the modal contents in Fig. 10, it is found that only the mode $nB + s_1V = -13$ ($s_1 = -3$) is cut-on upstream of the stator among the modes generated by the wake impingement, thus no sound is radiated downstream. The rotor is able to scatter this mode into $nB + s_1V + s_2B = 3$ ($s_2 = 1$), which is now cut-on in the entire stage and propagates noise downstream through the stator.

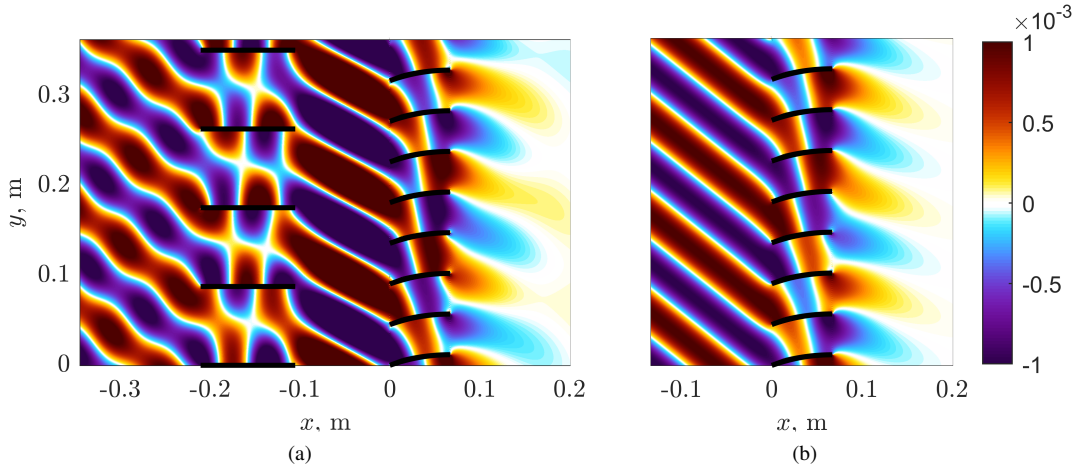

Fig. 9 Instantaneous pressure maps for the rotor-stator case (a) and the stator alone (b), with $n = 5$ and $M_\Omega \simeq 0.137$.

With a single stator, noise is only produced at the n^{th} BPF noise harmonic, in a one-to-one relationship with the incoming BPF wake harmonic. The scattering by the rotor redistributes noise upstream between the 5$^{\text{th}}$ BPF noise harmonic, carried by the mode -13 ($s_2 = 0$), and the 6$^{\text{th}}$ BPF noise harmonic, carried by the mode 3 ($s_2 = 1$). It also produces noise downstream at $6 \times$ BPF via the same mode 3. Figure 11 shows the distribution of Sound Power Level

Downloaded by Christophe Bogey on October 10, 2023 | http://arc.aiaa.org | DOI: 10.2514/6.2023-4189

(SWL) per BPF noise harmonic in both cases. The SWL is computed as SWL = $10\log_{10}\left(\mathcal{P}/\mathcal{P}_{ref}\right)$, with $\mathcal{P}_{ref}$ = 1 pW. In this case, the stator alone produces 125 dB upstream and nothing downstream. The rotor spreads an amount of the energy at the 5$^{\text{th}}$ BPF to the 6$^{\text{th}}$ BPF, resulting in 122 dB and 114 dB upstream, respectively, and 106 dB downstream.

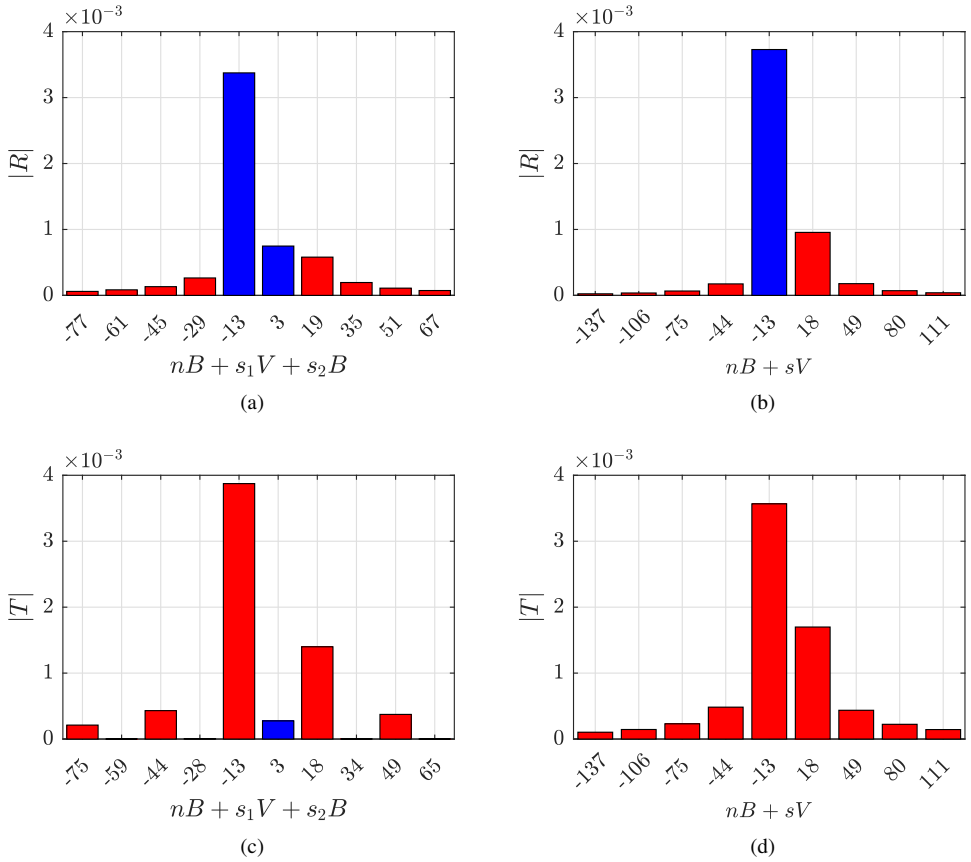

Fig. 10 Upstream and downstream modal contents for the rotor-stator case (a-c), and stator alone (b-d), with n = 5 and $M_\Omega \simeq 0.137$. Blue bars indicate cut-on modes, red bars are cut-off.

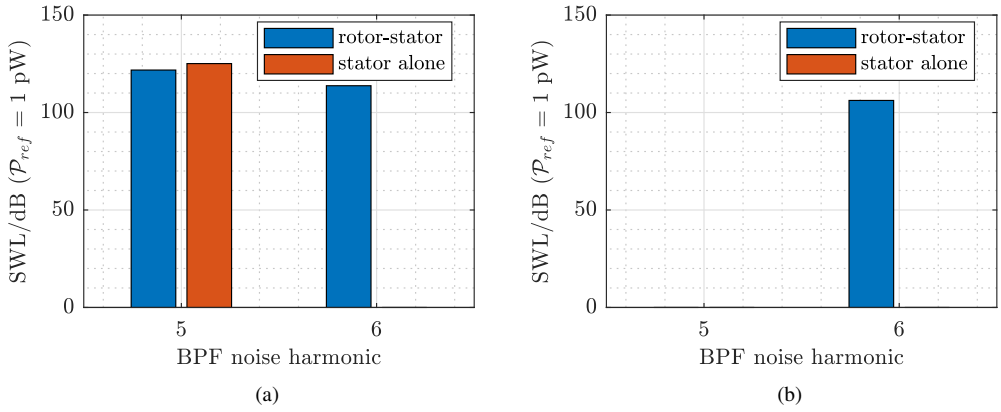

Fig. 11 Sound power levels radiating upstream (a) and downstream (b) for the rotor-stator and stator-alone cases, with n = 5 and $M_\Omega \simeq 0.137$.

Downloaded by Christophe Bogey on October 10, 2023 | http://arc.aiaa.org | DOI: 10.2514/6.2023-4189

Note that, due to the lack of mean flow deviation through the rotor in the current model, the flow conditions are the same in the inter-stage and upstream areas. This allows the mode -13 to propagate upstream, whereas it would be trapped with a purely axial upstream mean flow. This could be an interesting test case when adding stagger and camber to the rotor blades in the future.

Parametric studies are performed in the following to assess the impact of the rotor scattering with different inter-stage distances and rotor rotational speeds.

B. Parametric Studies

1. Inter-Stage Distance

The same test case is used but the inter-stage distance is increased from $d/l_2 = 1$ to $d/l_2 = 3$. The vortical amplitude $|u_i^R|$ at the stator leading-edge location is kept the same in both cases to emphasize on the effect of acoustic coupling, thus not accounting for the wake decay from the rotor TE to the stator LE. The real part of the resulting pressure map is plotted in Fig. 12 and the inter-stage modal content in Fig. 13. The strong interaction due to the mode -13 and its reflection is still visible.

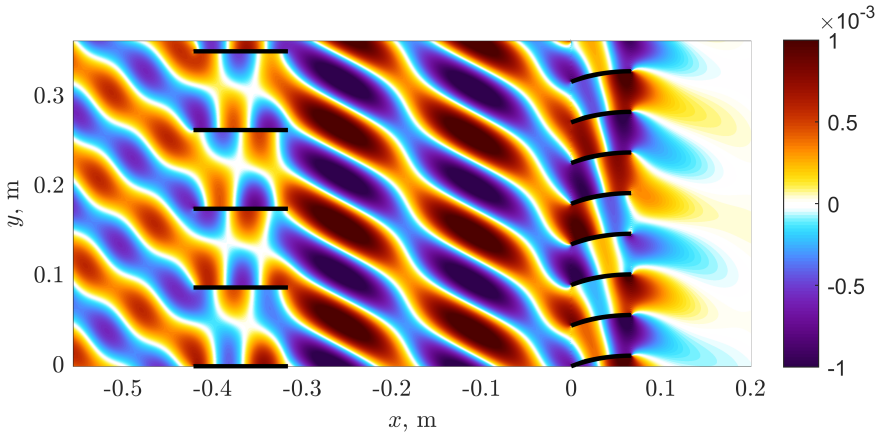

Fig. 12 Instantaneous pressure map for the rotor-stator case with $n = 5$, $M_\Omega \simeq 0.137$ and $d/l_2 = 3$.

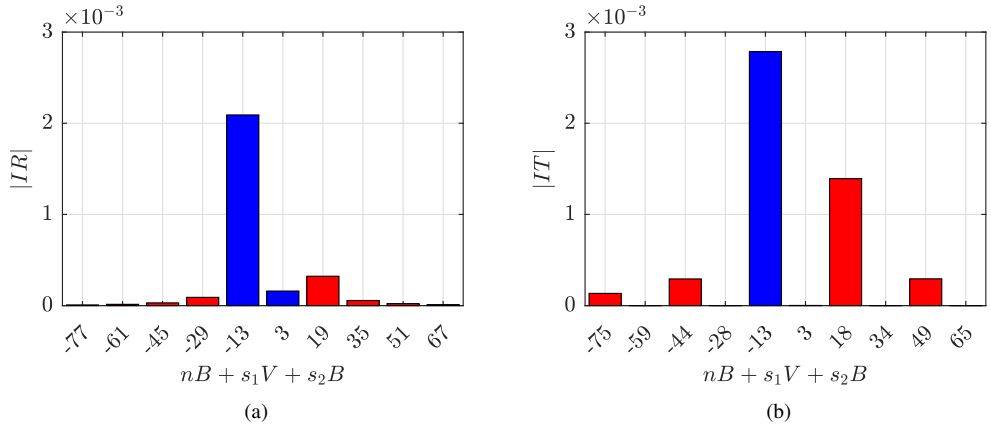

Fig. 13 Modal contents in the inter-stage propagating upstream (a) and downstream (b), with $n = 5$ and $M_\Omega \simeq 0.137$. Blue bars indicate cut-on modes, red bars are cut-off.

The incident disturbance is now changed to the third BPF wake harmonic $n = 3$ and the rotational Mach number is increased to $M_\Omega \simeq 0.188$. The wake-interaction in this case generates only cut-off modes as depicted in Fig. 14b. Adding the rotor at a close distance $d/l_2 = 1$ is able to scatter the cut-off mode $nB + s_1V = -14$ ($s_1 = -2$) before it

Downloaded by Christophe Bogey on October 10, 2023 | http://arc.aiaa.org | DOI: 10.2514/6.2023-4189

vanishes, hence spreading part of its energy to the cut-on mode $nB + s_1V + s_2B = 2$ ($s_2 = 1$) at the next noise harmonic $4 \times$ BPF. This can be seen in Fig. 14a.

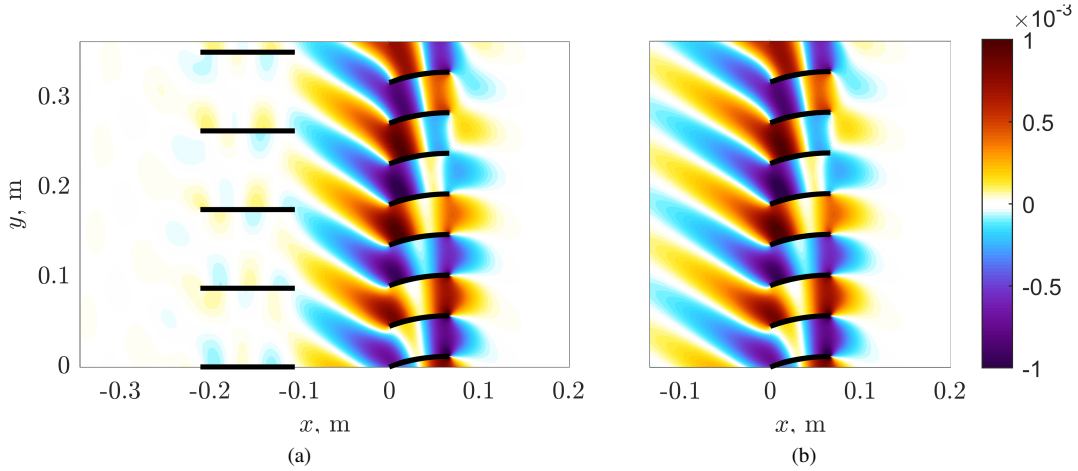

Fig. 14 Instantaneous pressure maps for the rotor-stator case (a) and the stator alone (b), with $n = 3$ and $M_\Omega \simeq 0.188$.

If the inter-stage distance is increased too much, the rotor and stator can no longer interact because of the exponentially decaying nature of the mode -14 produced by the stator. The Sound Power Levels (SWL) evolution per BPF noise harmonic is plotted against the inter-stage distance in Fig. 15b. The exponential decay of the noise radiating upstream and downstream is evidenced in this case. Notice that the downstream part is only visible at very small distances because of (i) the decrease in the reflection coefficient of the rotor and (ii) the threshold filtering of the algorithm. The previous case ($n = 5$ and $M_\Omega \simeq 0.137$) is also depicted in Fig. 15a. It is seen that both 5$^{\text{th}}$ and 6$^{\text{th}}$ BPF noise harmonics remain constant with d, demonstrating the noise levels does not depend upon the inter-stage distance if the interaction is due to cut-on modes with a fixed perturbation amplitude (independent to the distance d). In real applications, the velocity deficit is expected to decrease with the distance, thus the SWL in this case would decrease proportionally to the decaying prescribed velocity deficit. In conclusion, depending on the compressor design, cut-off modes could play a significant role on the radiated noise by energizing new tones. They should be accounted for in rotor-stator noise prediction tools.

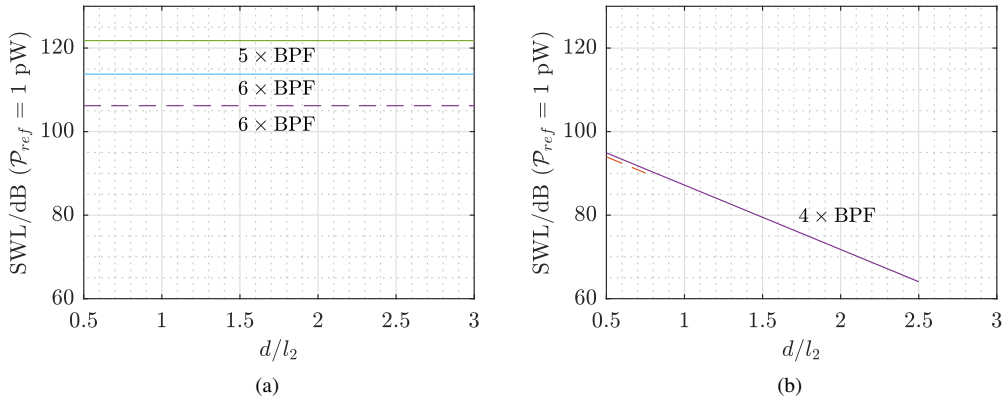

Fig. 15 Upstream (——) and downstream (– –) SWL per BPF harmonic with $n = 5$ and $M_\Omega \simeq 0.137$ (a), and $n = 3$ and $M_\Omega \simeq 0.188$ (b).

Downloaded by Christophe Bogey on October 10, 2023 | http://arc.aiaa.org | DOI: 10.2514/6.2023-4189

2. Rotor Rotational Mach Number

For this parametric study, the inter-stage distance is fixed to $d/l_2 = 1$ and now the rotor rotational speed varies. This increases the BPF, allowing more modes and tones to be produced. The first example is made with the 2nd BPF wake harmonic and a rotational Mach number ranging from 0.0171 to 0.222. Figure 16 shows the evolution of upstream and downstream SWL for the rotor-stator case and the stator alone. The radiated noise is dominated by the downstream field up to $M_\Omega \simeq 0.15$ in both cases, and is balanced for larger rotational speeds. The only difference when accounting for the rotor scattering is a decrease of 2 dB of the upstream power at the lowest rotational speed. This is attributed to the reflection of the stator noise by the rotor.

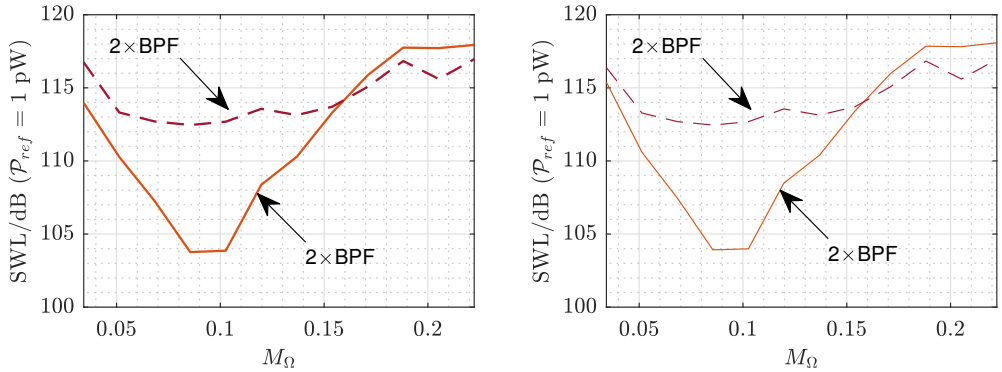

Fig. 16 Upstream (——) and downstream (– –) SWL per BPF harmonic with $n = 2$ for the rotor-stator case (a) and the stator alone (b).

When looking at higher wake harmonics, the pattern becomes more complex. Tones produced by the BPF wake harmonic $n = 5$ are displayed in Fig. 17. The stator alone (Fig. 17b) generates equivalent upstream and downstream noises at $5 \times$ BPF above $M_\Omega = 0.14$, and is silent below this value because the generated modes cannot propagate at theses frequencies. The rotor-stator case (Fig. 17a) displays evidences of frequency scattering by the rotor. The tone $6 \times$ BPF is generated at rotational speeds starting from 0.1, when the mode order 3 becomes cut-on, and the tone $7 \times$ BPF appears around 0.17 to 0.19, when the mode order 19 is able to propagate.

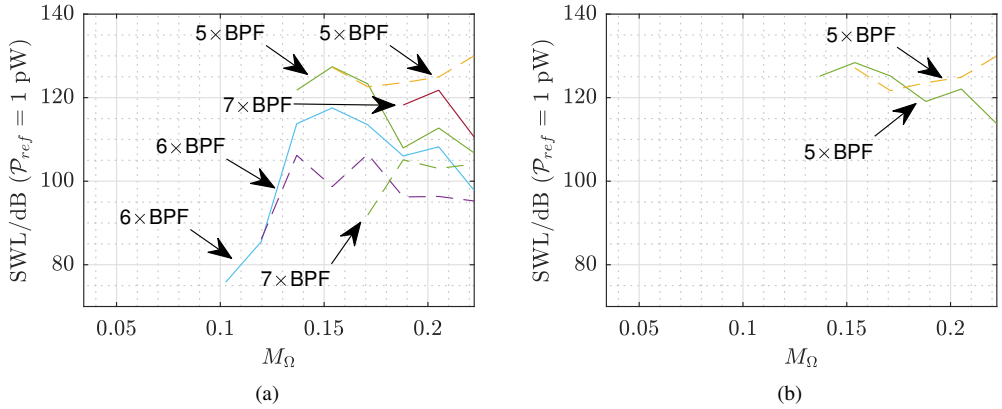

Fig. 17 Upstream (——) and downstream (– –) SWL per BPF harmonic with $n = 5$ for the rotor-stator case (a) and the stator alone (b).

The emerging 7th BPF noise harmonic has a significant impact on the noise produced at $5 \times$ BPF upstream of the compressor stage. Starting from $M_\Omega \simeq 0.19$, the tone $7 \times$ BPF completely replaces the tone $5 \times$ BPF when comparing

Downloaded by Christophe Bogey on October 10, 2023 | http://arc.aiaa.org | DOI: 10.2514/6.2023-4189

SWL with the stator alone scenario (Fig. 17b). This results in a sharp drop of 10 dB of the noise radiated upstream at $5 \times$ BPF. This shift of tonality is explained by the mode order 19 ($s_1 = -3$ and $s_2 = 2$) becoming cut-on between $0.171 \leq M_\Omega \leq 0.188$ and the energy distribution switching from the mode order -13 to 19, as shown in Fig. 18.

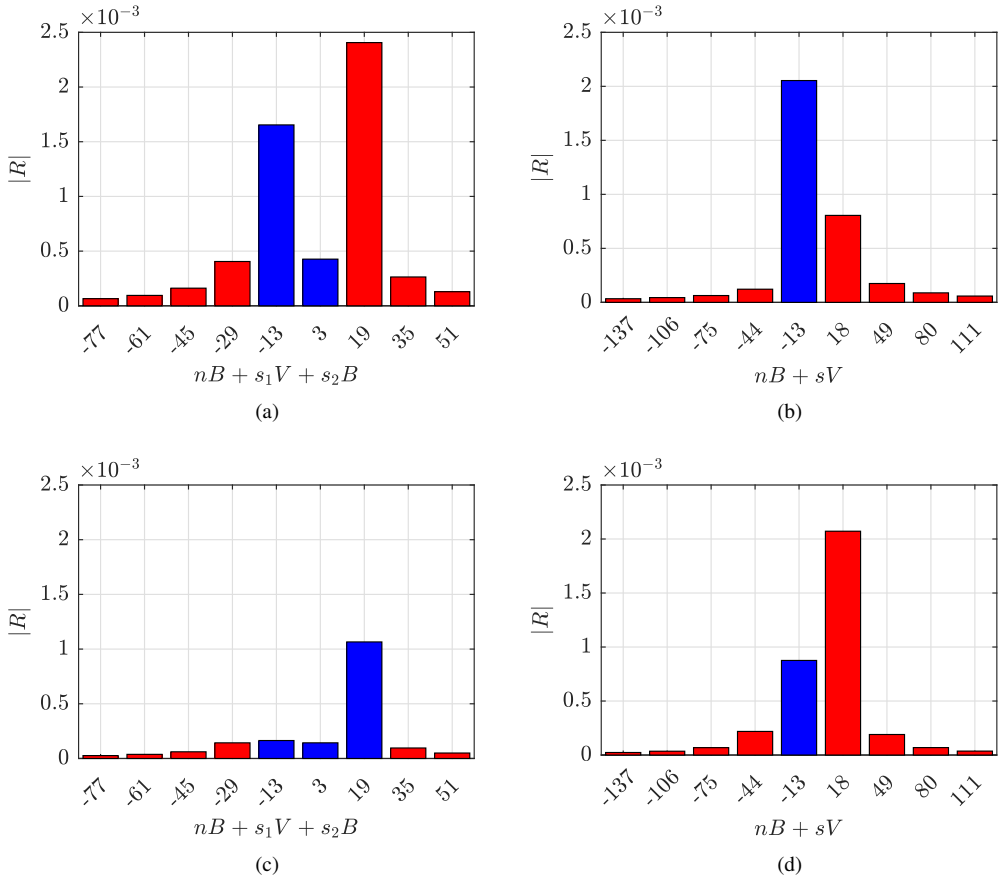

Fig. 18 Upstream modal contents at $M_\Omega \simeq 0.171$ and $M_\Omega \simeq 0.188$, respectively, with $n = 5$ for the rotor-stator case (a-c), and stator alone (b-d)

Finally, the pressure maps at both rotational speeds are presented in Fig. 19, in which the shift from the mode -13 to 19 is clearly observable in the upstream region.

To conclude on the effect of the rotor rotational speed on sound generation, the total noise produced by the first six BPF wake harmonics is studied. The acoustic powers carried by all modes, at all frequencies, generated by the first 6 wake harmonics are summed up together by virtue of linearity and plotted in dB in Fig. 20a. On the other hand, Fig. 20b displays the difference in dB between the upstream and downstream sound power levels as $\Delta\text{SWL} = \text{SWL}_{\text{up}} - \text{SWL}_{\text{down}}$. It is found that, in this case, adding the rotor increases the ratio downstream/upstream because of the reflection at the rotor trailing edge (so called "shielding" effect), which is stronger around $M_\Omega = 0.04$ and $M_\Omega = 0.15$ from Fig. 20b. However, the total power does not vary significantly between both cases in Fig. 20a. It seems that the work done by the rotor on the scattered waves demonstrated in section IV.B is either negligible in this case, or compensates itself by giving energy to some modes and taking to others. Section IV.B has shown power imbalances lower than 10% for this range of rotational speeds, which might lead to the conclusion that this effect is negligible here. Yet keep in mind that Fig. 20a is indeed for the total noise summed over all BPF noise harmonics. When looking at individual noise harmonics, significant discrepancies occur between the rotor-stator case and the stator alone.

Downloaded by Christophe Bogey on October 10, 2023 | http://arc.aiaa.org | DOI: 10.2514/6.2023-4189

Downloaded by Christophe Bogey on October 10, 2023 | http://arc.aiaa.org | DOI: 10.2514/6.2023-4189

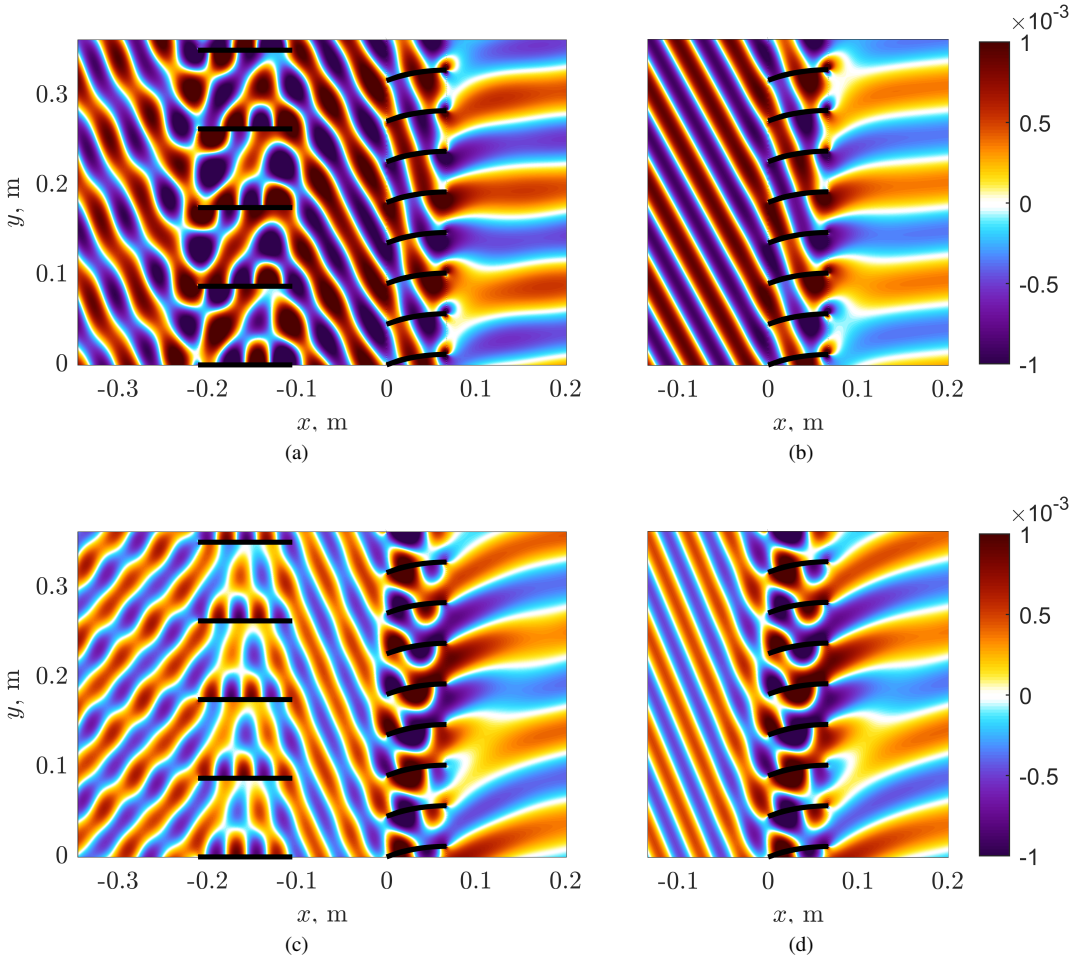

Fig. 19 Instantaneous pressure maps at $M_\Omega \simeq 0.171$ and $M_\Omega \simeq 0.188$, respectively, with $n = 5$ for the rotor-stator case (a-c) and the stator alone (b-d).

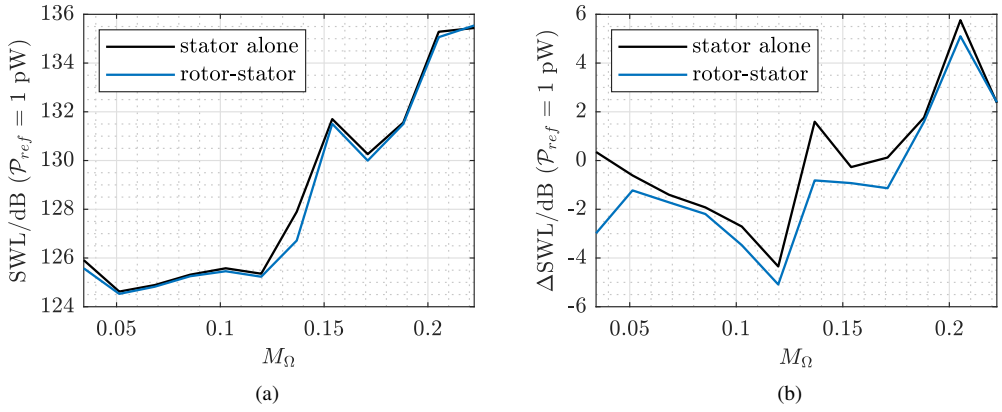

Fig. 20 Total sound power (a) generated by the first 6 BPF wake harmonics and the upstream-downstream difference in dB (b).

VI. Conclusion

A two-dimensional mode-matching technique for wake-interaction tonal noise has been developed, including rotor-stator coupling and the most recent achievements on mode matching in this context. The model consists of a primary sound generation computation by rotor wakes impingement on the stator, and then successive acoustic scattering iterations on the rotor and stator are performed until a convergence on the modal coefficients is reached. Thanks to previous works by the authors [10, 11], a continuous evolution of the mean-flow conditions is considered through the entire rotor-stator stage, and advanced geometrical design parameters such as stagger and camber are accounted for. The current version of the code runs in a few seconds on a personal computer for a given Fourier component of the wake mean-velocity deficit.

The consistency of the iterative procedure has been demonstrated on a stator-stator scenario with incident acoustic waves, which give access to a power balance. When an incident vortical wave is considered, only the "local" power balance at each iteration of acoustic scattering can be tracked. An estimation of the hydrodynamic power carried by the vortical wave could be implemented in a future work, based on Maierhofer & Peake's formulation [17] for example, to give further validations. It would also give guidance regarding the number of modes to account for in the modal truncation. Indeed, the radiated sound powers can be sensitive and simple convergence hard to obtain when camber is modeled, depending on the truncation [11]. Further comparisons with, for example, Hanson's results [4] and eventually experimental or numerical results with a hub-to-tip ratio close to unity is also something to aim for, in order to assess the physical consistency of the proposed model.

Acoustic power imbalances in presence of rotating scattering surfaces have been highlighted, which are in agreement with Hanson's theory [6]: an energy increase is found for modes scattered at higher frequencies and an energy decrease for modes scattered at lower frequencies. An exchange of energy between the acoustic field and the rotor is made possible by the conservation of the stagnation enthalpy in the rotating frame of reference, which is equivalent to the conservation of the rothalpy. Regarding the rotor-stator system, comparisons of radiated sound power levels between the rotor-stator system and a stator alone have shown expected outcomes: the rotor reflection generally increases the downstream to upstream power ratio and also redistributes power to a larger number of BPF noise harmonics due to frequency scattering, giving rise to tones that would not be present in a stator alone computation.

Concerning possible improvements of the current model version, the rotor blades geometry could benefit from the improvements made for the stator. Staggered and cambered blades would enable different flow conditions between the inter-stage and upstream areas, thus being more realistic and favoring the occurrence of trapped modes, which was not accessible in the current study.

The methodology could be extended to three dimensions without difficulty, only at the cost of a higher computation time. Hanson [18–20] treated turbulence impingement noise on the stator with full unsteady rotor-stator coupling. He showed that accounting for the rotor-stator coupling can lead to a substantial increase of the noise radiated downstream and a decrease of the noise radiated upstream of the compressor stage. Accounting for the fully coupled system instead of an isolated stator seems mandatory for reliable noise predictions and the mode-matching model presented herein could be extended to broadband noise in that purpose. Hanson also explained how scattered modes spread over limited mode subsets, thus reducing the possibilities of coupling. This principle of independent mode subsets, as well as considerations in frequency truncation explained in Ref. [20], could help to build an efficient broadband noise prediction strategy.

Downloaded by Christophe Bogey on October 10, 2023 | http://arc.aiaa.org | DOI: 10.2514/6.2023-4189

Acknowledgments

This work was performed within the framework of the industrial chair ARENA (ANR-18-CHIN-0004-01) co-financed by Safran Aircraft Engines and the French National Research Agency (ANR), with the help of the French governmental plan "France Relance", and is also supported by the Labex CeLyA of the Université de Lyon, operated by the French National Research Agency (ANR-10-LABX-0060/ANR-16-IDEX-0005).

References

[1] Huber, J., and Illa, S., "Jet noise assessment and sensitivity at aircraft level," *13th AIAA/CEAS Aeroacoustics Conference*, Rome, Italy, 2007.

[2] Topol, D. A., Holhubner, S. C., and Mathews, D. C., "A reflection mechanism for aft fan tone noise from turbofan engines," *11th Aeroacoustics Conference*, Sunnyvale, CA, U.S.A., 1987. https://doi.org/10.2514/6.1987-2699.

[3] Hanson, D. B., "Mode trapping in coupled 2D cascades - Aerodynamic and acoustic results," *15th Aeroacoustics Conference*, Long Beach, CA, U.S.A., 1993. https://doi.org/10.2514/6.1993-4417.

[4] Hanson, D. B., "Coupled 2-Dimensional Cascade Theory for Noise and Unsteady Aerodynamics of Blade Row Interaction in Turbofans. Volume 1-Theory Development and Parametric Studies," Contractor Report NASA-CR-4506, NASA, 1994.

[5] Smith, S. N., "Discrete frequency sound generation in axial flow turbomachines," Reports and Memoranda 3709, Aeronautical Research Control Council, 1972.

[6] Hanson, D. B., "Acoustic reflection and transmission of rotors and stators including mode and frequency scattering," *3rd AIAA/CEAS Aeroacoustics Conference*, Atlanta, GA, U.S.A., 1997. https://doi.org/10.2514/6.1997-1610.

[7] Bouley, S., François, B., Roger, M., Posson, H., and Moreau, S., "On a two-dimensional mode-matching technique for sound generation and transmission in axial-flow outlet guide vanes," *Journal of Sound and Vibration*, Vol. 403, 2017, pp. 190–213. https://doi.org/10.1016/j.jsv.2017.04.031.

[8] Bouley, S., "Modélisations analytiques du bruit tonal d'interaction rotor / stator par la technique de raccordement modal," Phd thesis, Université de Lyon, 2017. URL http://www.theses.fr/2017LYSEC007.

[9] Oulmi, M., Roger, M., and Boualem, B., "Analytical Modelling of Sound Transmission Through a Row of Thick-walled Channels," *eForum Acusticum*, Lyon, France, 2020, pp. 371–377. https://doi.org/10.48465/fa.2020.0498.

[10] Girier, L., Roger, M., Bériot, H., Lafitte, A., and Posson, H., "A Two-Dimensional Model of Sound Transmission Through Curved and Staggered OGV: Effect of Inter-Vane Channel Mode Transitions," *25th AIAA/CEAS Aeroacoustics Conference, AIAA Paper 2019-2690*, Delft, The Netherlands, 2019. https://doi.org/10.2514/6.2019-2690.

[11] Girier, L., "Mode-matching techniques for the modeling of rotor-stator wake-interaction noise, with emphasis on the effects of vane camber," Phd thesis, Université de Lyon, 2022. https://doi.org/10.13140/RG.2.2.26992.74241.

[12] Oulmi, M., Roger, M., Boualem, B., and Trahard, Q., "Sound Generation and Propagation in a System Consisting of Two Periodic Rows of Channels," *FAN 2022*, Senlis, France, 2022. https://doi.org/10.26083/tuprints-00021690.

[13] Oulmi, M., "Analytical Modelling of the Aeroacoustic Performances of Self-ventilated Motors Used in Railway Applications," Phd thesis, Université de Lyon, 2022.

[14] Dixon, S. L., and Hall, C. A., *Fluid Mechanics and Thermodynamics of Turbomachinery*, 7^{th} ed., Elsevier, 2014.

[15] Chu, B.-T., and Kovásznay, L. S. G., "Non-linear interactions in a viscous heat-conducting compressible gas," *Journal of Fluid Mechanics*, Vol. 3, No. 5, 1958, pp. 494–514. https://doi.org/10.1017/S0022112058000148.

[16] Goldstein, M. E., *Aeroacoustics*, McGraw-Hill International Book Co., New York, 1976.

[17] Maierhofer, G., and Peake, N., "Acoustic and hydrodynamic power of wave scattering by an infinite cascade of plates in mean flow," *Journal of Sound and Vibration*, Vol. 520, 2022, p. 116564. https://doi.org/10.1016/j.jsv.2021.116564.

[18] Hanson, D. B., "Broadband Noise of Fans - With Unsteady Coupling Theory to Account for Rotor and Stator Reflection/Transmission Effects," Contractor Report NASA-CR-2001-211136, NASA, 2001.

[19] Hanson, D. B., "Broadband Theory for Coupled Fan Stages Including Blade Row Reflection/Transmission Effects," *8th AIAA/CEAS Aeroacoustics Conference and Exhibit*, Breckenridge, Colorado, 2002. https://doi.org/10.2514/6.2002-2488.

[20] Hanson, D. B., "Broadband Noise Source Studies for a Fan with a Coupled Rotor/Stator," *9th AIAA/CEAS Aeroacoustics Conference and Exhibit*, Hilton Head, South Carolina, 2003. https://doi.org/10.2514/6.2003-3132.

Downloaded by Christophe Bogey on October 10, 2023 | http://arc.aiaa.org | DOI: 10.2514/6.2023-4189